Slippery and Sticky Graphene in Water

2	Yijue Diao ^{1§} , Gus Greenwood ^{1§} , Michael Cai Wang ² , SungWoo Nam ² ,
3	Rosa. M. Espinosa-Marzal* ¹
4	1 Department of Civil and Environmental Engineering, University of Illinois at Urbana-
5	Champaign, 205 N. Matthews Avenue, Urbana, IL 61801, United States.

2 Department of Mechanical Science and Engineering, University of Illinois at Urbana-

Champaign, 1206 W. Green St., Urbana, IL 61801, United States

Abstract

Understanding modulation of water molecule slippage along graphene surfaces is crucial for many promising applications of two-dimensional materials. Here, we examine normal and shear forces on supported single-layer graphene supported by Atomic Force Microscopy and find that the composition of the electrolyte composition affects the molecular slippage of nanometer thick films of aqueous electrolytes along the graphene surface. In the light of the shear-assisted thermally activated theory, water molecules along the graphene plane are very mobile when subjected to shear. However, upon addition of an electrolyte, the cations can make water stick to graphene, while ion-specific and concentration effects are present. Recognizing the tribological and tribochemical utility of graphene, we also evaluate the impact of this behavior on its frictional response in the presence of water. Further, this work can inspire innovation in research areas where

- 20 changes of the molecular slippage through the modulation of the doping characteristics of graphene
- 21 in liquid environment can be of use, including molecular sensing, lubrication and energy storage.
- **Keywords:** graphene, water, electrical double layer, stress-promoted thermally activated slip,
- 23 molecular slippage, friction.
- With pristine graphene¹⁻² being a gapless and semimetallic material, it has been found to exhibit
 many unique properties including ballistic electron transport,³ large in-plane elastic modulus⁴ and
 low coefficient of friction.⁵ Graphene is seen as a potential coating material to control friction at
 interfaces due to its crystallinity, which allows achieving "structural superlubricity" due to the
 incommensurability between misaligned graphene sheets.⁶⁻⁷ However, water is ubiquitous and
 often the origin of failure of electro-mechanical devices due to the relevance of interfacial forces
 like adhesion and stiction between moving components. Strategies to modulate interfacial forces
- 31 will help meet future structural and functional requirements of such devices.
 - Intrinsically, graphene is hydrophilic with a water contact angle of ~45°, 8-9 but hydrocarbonaceous adsorbates of ambient origin may impart hydrophobicity to graphene. 8-10 The effect of water on graphene friction has been demonstrated in several works, 11-15 but the underlying mechanisms are only partially understood. For instance, density functional theory (DFT) calculations demonstrated that one monolayer of water broadens the spectral range of graphene vibrations. This effect provides new excitation channels and increases the overlap with the atomic vibrations of the substrate, both facilitating coupling and energy transfer, and thereby leading to an increase in friction. 15 The importance of liquid slippage on the viscous shear force and the friction between sliding solid surfaces has been often acknowledged. 16-18 In this context, molecular dynamics (MD) simulations 14 found that friction is higher in humid air than under vacuum. More

importantly, the authors attributed the observed friction hysteresis during loading (increase in load) and unloading (decrease in load) to the energy dissipated by the motion of the liquid molecules along the graphene surface and the pinning of water to the surface (in the absence of defects) – which resulted in a contact angle hysteresis— thereby showcasing the relevance of molecular slippage in dictating friction. Along this line, it is well-accepted that the low friction coefficient provided by graphite in humid environment stems from the water trapped between graphene sheets, which facilitates interlayer slip. ¹⁹ In contrast, ab initio simulations ²⁰ have recently showed that water can escape from the interlayer space to react with graphene edges, emphasizing the relevance of water slippage on the lubrication mechanism and the discrepancy of results.

The discovered ultrafast water slippage in carbon nanotubes and graphene nanochannels²¹⁻²³ is a matter of scientific and technological interest but the lack of complete understanding still limits the development of graphene-based nanofluidic devices and separation membranes that enable control of flow. It is well-accepted that the slip length -defined as the ratio between the viscosity and the interfacial friction between the liquid molecules and the solid surface- is strongly related to the contact angle, which mainly stems from the effect of interaction energy between the solid and the liquid molecules on slippage.²⁴ To the authors' knowledge only one experimental work has reported values for the slip length of water on graphene ranging from ~0 to ~200 nm, with a most frequent value ~16 nm.²⁵ The large variation of the slip length was attributed to the variation of the graphene's surface charge and the interactions between graphene and the silica substrate based on MD simulations. Higher slip lengths (~60 nm) have been obtained by MD simulations in separate works.²⁶⁻²⁷

The focus of this work is to experimentally investigate the molecular slippage of films of nanometer thickness of water and aqueous electrolytes along graphene surfaces and its effect on

graphene friction. Monolayer graphene was synthesized via low-pressure chemical vapor deposition on 25µm copper foils using methane as the precursor with hydrogen/argon carrier gas, as previously documented.²⁷ The graphene was transferred onto ~285 nm thick thermally-grown silicon oxide on silicon wafers using polycarbonate handle layers by solution etching of the copper substrate. As-prepared samples were subsequently annealed at 500°C in a hydrogen/argon environment to improve graphene-substrate adhesion and to remove surface and interfacial polymeric residue immediately prior to measurements. Normal and lateral force measurements were conducted on graphene samples with an Atomic Force Microscope (AFM) using silicon tips in defect-free regions far away from boundaries after ensuring the absence of "pucker-up" effects.²⁸ Further details about the methods used can be found in the Methods section. The force measurements reveal an electrical double layer on graphene and ion specific effects when comparing the results in ultrapure water, KCl and NaCl solutions. We also resolve the structure of nanometer thick thin films confined between graphene and the AFM tip with subnanometer resolution through the analysis of the disjoining pressure, and interrogate the influence of the selected electrolytes on the friction force from the perspective of the stress-assisted thermally activated slip theory.²⁹ This evaluation provides the effect of the electrolyte composition on the molecular slippage in thin films by considering that slip is a rate process, 30-32 where the hopping of the liquid molecules from an energetically stable position to the adjacent one along the slip plane is promoted by the applied shear force at the interface, which helps overcoming the required energy barrier. The results demonstrate that tuning the ionic composition of the aqueous phase is a means to modulate molecular slippage and friction.

86

85

65

66

67

68

69

70

71

72

73

74

75

76

77

78

79

80

81

82

83

84

Results

88

89

90

91

92

93

94

95

96

97

98

99

100

101

102

103

104

105

106

107

108

109

110

The electrical double layer of graphene in aqueous environment

The force acting between the AFM tip and graphene (see schematics in Figures 1a) was measured in ultrapure water and in NaCl and KCl aqueous solutions with concentrations ranging between 1mM and 1 M and at an adjusted pH of 6, while approaching the tip to the surface at a constant velocity of 20 nm s⁻¹. All the measurements were conducted in the absence of any bias potential. Figures 1b-c show representative results in water and in NaCl solutions, respectively. The results for KCl can be found in Figure S1. In water, the surface force between tip and graphene is repulsive and exponentially decaying (Figure 1b, pH 6), and it becomes attractive at separations D smaller than ~4 nm. By increasing the NaCl concentration, the decay length of the exponentially decaying repulsive force decreases and it agrees well with the expected Debye length of monovalent ions at concentrations ≤100mM, which indicates that the origin for this long-range repulsion is an electrical double layer force. Moreover, control tests at 50°C confirm that the decay length scales with $T^{1/2}$, as expected for the Debye length of an electrical double layer. ²⁸ Detecting an electrical double layer repulsion is a key result because it indicates that graphene behaves as effectively charged in aqueous environment. To provide more insight into the electrical double layer, the force-distance curves were modeled according to the Derjaguin-Landau-Verwey-Overbeeck (DLVO) theory at separations larger than ~3 nm, using the electrostatic potential at a plane, the outer Helmholtz plane (OHP), located a few Angstroms above the graphene surface (beyond which the ions are mobile), as one of the model parameters.²⁸ Details of the DLVO model can be found in the SI. To demonstrate that the tip is negatively charged, force measurements were also conducted on a (negatively charged) mica surface in pure water and on a polycationic film of nanometer thickness (Figure S2). The attraction of the tip to the polycationic film and the repulsion away from the (negatively charged) mica surface reveal the negative charge of the tip under all solution conditions. Normal force measurements were also conducted on a (naturally oxidized) silicon wafer with a (naturally oxidized) silicon AFM tip to unambiguously determine the magnitude of the OHP potential of silicon dioxide surfaces, tip and substrate (Figures S3-S4). With the known OHP potential of the AFM tip, the fit of the DLVO equation to the experimental results on the graphene surface provides the OHP potential of graphene (ϕ_G), as shown in Figure 1d-e; the surface charge of graphene is roughly estimated from $\sigma_G = \varepsilon \varepsilon_0 \kappa \phi_G$, κ^{-1} being the Debye length, and $\varepsilon \varepsilon_0$ the permittivity of water,²⁸ for comparison to literature values.

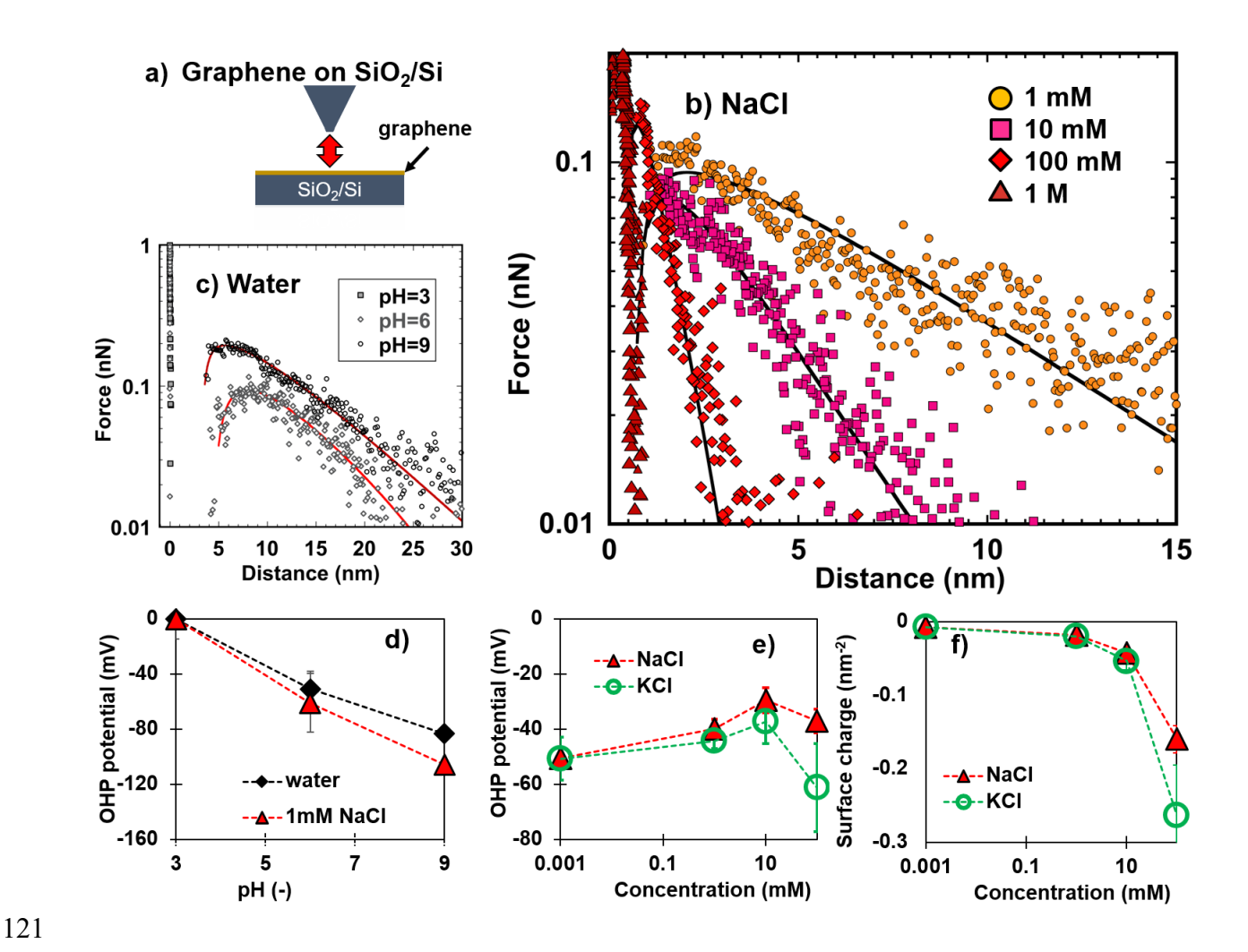


Figure 1. Surface force between graphene and the silicon tip in aqueous environment. **(a)** Schematic representation of the experimental setup where the AFM tip approaches to the graphene surface to measure normal forces. **(b)** Force between graphene and an AFM tip in DI water (different symbols represent measurements at pH 3, 6 and 9), and **(c)** in NaCl solution at the concentrations of 1 mM (circles, orange), 10 mM (squares, magenta), 100 mM (diamonds, red) and 1M (triangles, dark red). The radius of the tip is 50 nm. The surface potential of the tip obtained from control measurements (Figure S3c) is: -123(7) mV in water, -122(9) mV (1mM), -126(5) mV (10mM) and -57(13) mV (100 mM) at pH 6, and at pH 9, it is: -122(9) mV and -154(14) mV in

water and in 1mM NaCl, respectively. OHP charge of graphene obtained by fitting Eq. S1 to the experimental results in (d) water and 1mM NaCl at different pH values and (e) in KCl and NaCl solutions as a function of the concentrations at pH of 6, and (f) calculated surface charge with the Grahame equation. The error bars show the standard deviation of fitting 8-10 force-distance curves. Although the graphene charge in water appears to be \sim 0 at the selected scale of the Y-axis, the value is small and negative, $\sigma_G \sim 0.008(0.001)$ nm⁻². The zero separation was assumed to be the hard wall at the applied force of 5 nN (2 GPa).

The fit is very good under all conditions (lines in Figures 1 b-c and S1). The OHP potential of the tip remains negatively charged in the selected solutions (see caption of Figure 1), in agreement with reported results for silicon oxide,²⁹ and hence, the repulsive force in Figure 1c indicates that graphene acts as negatively charged under all conditions; see the obtained OHP potential in Figure 1d-e. The effective charge of graphene (Figure 1f) becomes more negative with gradual addition of salt and the difference in magnitude between NaCl and KCl solutions becomes more pronounced with increasing concentration, indicating that ion-specific effects become more relevant; *e.g.* the surface charge of graphene in 100 mM NaCl and KCl solutions is -0.16 nm⁻² and -0.26 nm⁻², respectively.

In pure water, we find that graphene exhibits a small negative charge, $\sigma_G \sim -0.008$ nm⁻². Force measurements as a function of the pH in water support that H⁺ adsorb on graphene and counterbalance the surface charge at sufficiently high concentration (*i.e.* low pH). Figure 1b shows that at the lowest tested pH value of 3, the double layer repulsion completely vanishes, which indicates that the adsorbed ions completely compensate the surface charge. In contrast, the electrical double layer repulsion becomes stronger at pH of 9 due to the higher graphene OHP

potential. The preferential adsorption of H⁺ compared to Na⁺ and K⁺ (see binding energies in ref.³⁰) can thus justify the small surface charge of graphene in ultrapure water compared to NaCl and KCl. Increasing the salt concentrations (≤ 10 mM) does not lead to a remarkable change of the OHP potential, indicating that the Stern layer composition does not vary significantly for the two salts. This suggests that hydronium still outcompetes K⁺ and Na⁺ ions and majorly adsorbs onto graphene. At a concentration of 100 mM, in contrast, the OHP potential abruptly decreases, especially in the case of KCl, which implies the prominent change of the Stern layer. A similar behavior has been reported for mica and attributed to the competitive adsorption of hydronium and (hydrated) metal cations to the surface. 31-33 Here, strongly hydrated metal cations remain further away from the surface surrounded by water molecules and balance the surface charge of mica less efficiently than hydronium, which causes the OHP potential to become more negative. It was observed that, because Na⁺ ions are more strongly hydrated than K⁺ ions, higher concentrations are needed for the Na⁺ ions to replace the H⁺ at the mica/solution interface.³¹ It is, therefore, possible that competitive adsorption also happens on graphene and that the K⁺ ions replace H⁺ already in 100 mM KCl solutions, whereas a higher concentration is required in the case of NaCl, leading to the observed change in OHP potential. In fact, MD simulations have showed that K⁺ ions adsorb more strongly to graphene than Na⁺ at high concentrations (1 M).³⁴ This is also supported by the results of the interfacial structure discussed next. Reported values of the surface charge of CVD graphene supported on Si/SiO₂ span over three orders of magnitude and are smaller than ~-0.2 nm⁻², ²⁵ and hence, our values are in the reported range. The origin of the negative surface charge of graphene deserves discussion. A few works

have proposed the negative surface charge to arise from residue adsorption related to the sample

153

154

155

156

157

158

159

160

161

162

163

164

165

166

167

168

169

170

171

172

173

174

preparation.³⁵ However, the reproducibility of the data across different graphene samples and the agreement of the experimental results in ultrapure water before and after the measurements in the electrolyte solutions let us exclude adventitious contamination as a source of the surface charge. First-principle DFT calculations have demonstrated that π -ion interactions lead to ion adsorption on graphene from the aqueous phase³⁴ and experiments corroborate that ions adsorb on graphene in contact with a liquid electrolyte. 30, 36 Cation adsorption would render positive surface charge to graphene, which would lead to an attractive double layer force, thereby contradicting our results. Anion adsorption thus appears as a potential charging mechanism, ³⁷ with higher amount of anions adsorbing at higher chloride concentration. However, several works consider K⁺ and Na⁺ to adsorb more preferentially on graphene than Cl⁻³⁰ To test this, control force measurements at three different pH-values in water and in 1mM NaCl were carried out (see Figure 1b and Figure S5 in the SI). The results confirm that the changes in hydronium (H⁺) concentration dictate the surface potential and not the chloride concentration, which let us exclude anion adsorption as the charging mechanism. While we cannot exclude the presence of a small density of oxygen functional groups on CVD graphene that could render the surface negatively charged, 25 about ~10% of the surface silanol groups of the SiO₂ substrate underneath graphene can ionize during the transfer of graphene in water at pH ~6, which could yield a maximum substrate charge of ~-0.6 nm⁻².38 The largest graphene charge σ_G is ~-0.26 nm⁻² (1 negative charge every 2 nm), and therefore, the charge of the underlying silica oxide substrate combined with partial screening by the graphene³⁹⁻⁴⁰ could be responsible for the charge of the graphene surface, as well.

Interfacial nanostructure

When the AFM tip is slowly approached to the surface, ions and water are squeezed out and the remaining molecules rearrange in the films confined by the solid surfaces. When the distance (D)

176

177

178

179

180

181

182

183

184

185

186

187

188

189

190

191

192

193

194

195

196

197

between tip and graphene becomes smaller than ~3 nm, a stronger repulsion with superposed steps is measured (see arrows in Figure 2 for NaCl and Figure S6 for KCl). This short-range repulsion between the confining walls (also called disjoining force or pressure) is originated not only by dispersion and electrostatic interactions but it is also affected by the adsorption of the molecules to the surfaces and by structural (or layering) effects of the thin films of nanometer thickness.⁴¹ On atomically flat surfaces, like graphene, the liquid molecules tend to arrange in layers. When the tip approaches the surface, it jumps from one to the next layer, 42 which appears as a step in the force-separation curve. This means that layers of water and ions located close to the graphene surface are probed by the tip. The size of the steps gives roughly the thickness of the interfacial layers of ions and water. The inset in Figure 2a displays a bubble diagram of the step size measured in water (black) and in the NaCl (red) and KCl (green) solutions, where the bubble size gives the relative frequency of the steps of this size. In water, the thickness of the steps is of the size of the water molecule, $\sim 2.7(0.3)$ Å. The presence of Na⁺ ions is reflected in an increase of the step size from $\sim 2.7(0.3)$ to ~ 4.5 Å (yellow region) and 7.4 Å (blue region) in 1mM NaCl solution, which indicates that ions (with their hydration shells) populate the interfacial region, along with water, as also observed in SFA experiments with mica elsewhere. 31, 43 The small size of the steps displaced at the highest forces (~3.1 Å, grey region) suggests that water is still present at the graphene/NaCl solution interface. Increasing the NaCl concentration leads to a progressive decrease in the step size, indicating that layers with less hydrated ions are probed with the tip at higher concentrations, but water is always present close to the graphene surface and removed at the highest applied pressures (see the red bubbles in the grey region). The structure of the thin films felt by the tip in KCl is different. The smaller size of the steps (3-4 Å, yellow region) indicates that the tip probes layers rich in ions but

199

200

201

202

203

204

205

206

207

208

209

210

211

212

213

214

215

216

217

218

219

220

less hydrated than in the case of Na⁺ as inferred from their smaller size. Further, the absence of steps in the range 2-3 Å (grey region) suggest that K⁺ ions has displaced interfacial water layers, so that they interact more directly with the graphene surface. Note that Na⁺ is a strongly hydrated cation with multiple near-surface hydration states, while K⁺ has a lower hydration strength.⁴⁴-Thus, the measured interfacial structure is consistent with MD simulations of the graphene/electrolyte interface, which show that ions with high hydration strength (*e.g.* Na⁺) might not penetrate through the interfacial water layers, while larger ions (*e.g.* Rb⁺ or K⁺) can dehydrate and interact more closely with graphene.⁴⁵

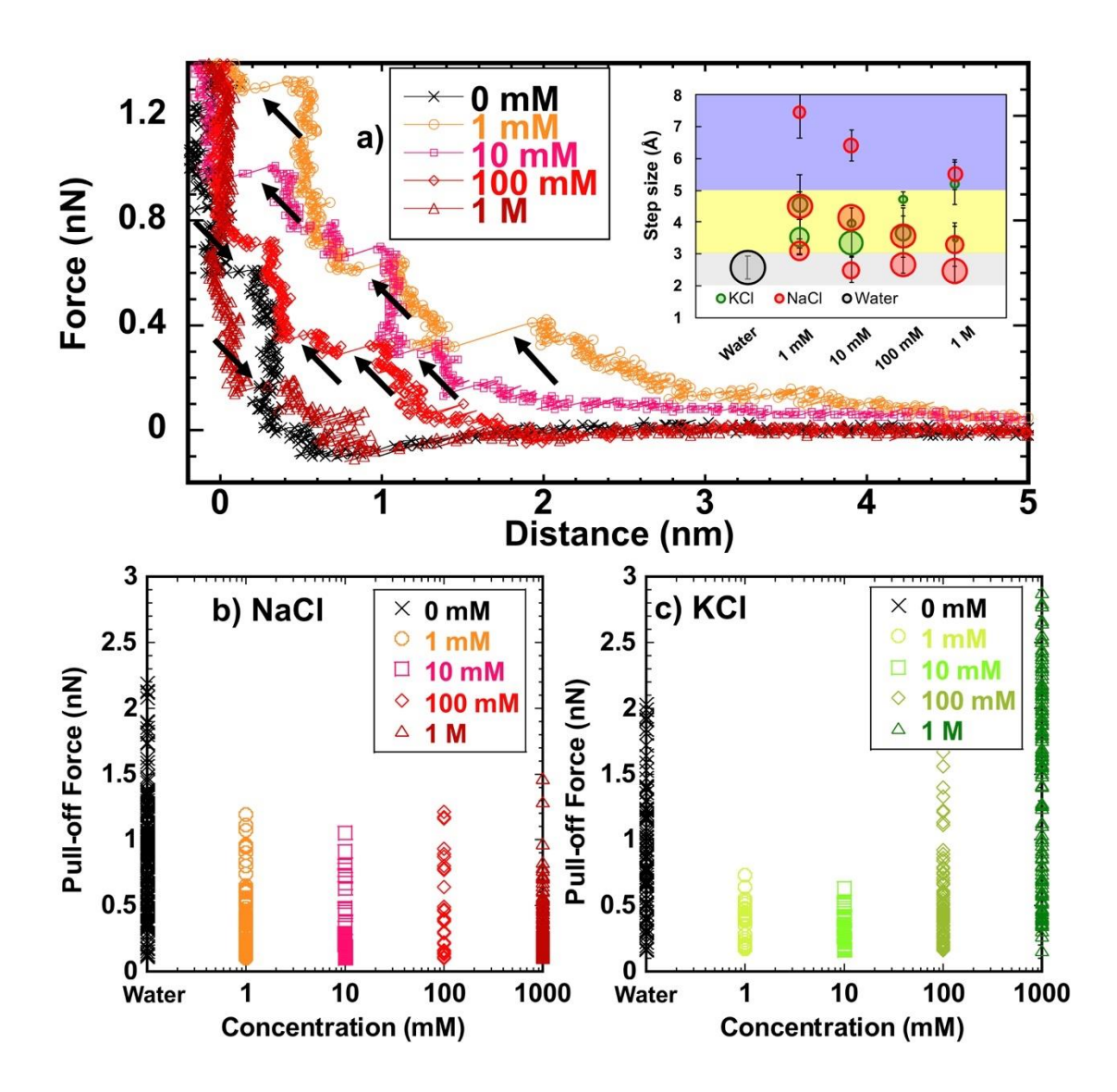


Figure 2. Structure of the graphene-electrolyte interface. **(a)** Short-range surface force as a function of the separation between the silicon tip and graphene in water (0 mM) and NaCl solutions. The inset shows a bubble diagram of the step size in NaCl (red) and KCl (green) solutions as a function of the concentration and in water (black). The size of the bubble is proportional to the frequency of the steps with this size. Three regions are distinguished with shades: 2-3 Å (grey), 3-5 Å (yellow) and 5-8 Å (blue). **(b-c)** Pull-off force as a function of the concentration in b) NaCl and c) KCl solutions. Radius of the tip is 50 nm.

At pressures above 1 GPa, no more layers are resolved, and therefore, the composition of the thin films cannot be further examined. Due to the uncertainty about the location of the absolute separation in AFM experiments, the true thickness of the confined liquid film cannot be precisely determined. Nevertheless, previous experiments¹² and MD simulations¹⁴ showed that a pressure higher than ~13 and 30 GPa, respectively, needs to be applied to squeeze-out the water trapped between a tip and graphene, independently of the assumed hydrophilicity of the graphene surface. This range of pressures is ~4-10 times larger than the maximum value applied in our experiments to prevent the damage of the tip. Although the composition of this thin film cannot be examined by squeezing out layers, its impact on adhesion and on the shear force can be investigated by measuring the pull-off force and the friction force, respectively.

Figures 2b and 2c summarize the pull-off force that is measured when the tip is retracted from the surface. The addition of 1mM KCl and NaCl decreases the pull-off force to the half (\sim 1.5(0.5) nN in water). A change in the pull-off force is observed in KCl solutions, first decreasing and then increasing at concentrations \geq 100 mM, while this increase happens at \geq 1 M in the case of NaCl and it is much less prominent. This different behavior reflects the effect of the different composition of the confined fluid film on adhesion. The pull-off force is reduced with respect to

its value in air (~5 nN),⁵ due to reduced van der Waals (dispersion) forces (see Hamaker constant in the SI).

In theory, the adhesion energy between two solid surfaces in an electrolyte solution has dispersive, structural and electrostatic contributions.²⁸ Obviously, the distance between the surfaces increases when the thickness of the confined liquid film is greater, which decreases the dispersive contribution (van der Waals) to the adhesion energy. The layered structure of the fluid film leads to multiple adhesive minima that are less strongly adhesive than the adhesion between the solid surfaces. This may justify the decrease in the pull-off force in the electrolyte solutions (with more layers) compared to ultrapure water, as reported for other systems.²⁸ At high concentrations, the electrostatic contribution originating from ion-ion correlations becomes more significant. 46 Here, an excess of counterions on one side is correlated with a lack of counterions on the opposite side, causing an overall attraction, and an increase in adhesion energy. It is thus possible that ion-ion correlations become significant for KCl at concentrations above 10 mM, when the pull off force is seen to increase, while in the case of NaCl, they become relevant only at concentrations ~1 M. This different behavior of the two electrolytes is supported by the higher amount of interfacial water in the NaCl thin films that was inferred from the size of the layers (inset in Figure 2b). Note that a similar trend was observed for NaNO3 and KNO3 when confined between mica surfaces, ^{31,43} and hence, this behavior is not unique to graphene.

273

274

275

276

277

255

256

257

258

259

260

261

262

263

264

265

266

267

268

269

270

271

272

Friction between a silicon tip and graphene in aqueous environment

Friction was first measured as a function of normal load at constant sliding velocity of 0.2 μm s⁻¹ (Figure 3) by increasing the applied normal load stepwise (loading curve, empty circles) and then decreasing (unloading curve, filled diamonds). Friction increases first in a linear fashion until an

abrupt increase is observed at ~60 nN (Hertzian stress~10 GPa). While this sudden increase in friction could indicate the onset of wear, the low friction was recovered in the unloading curve, thereby demonstrating the reversibility of the mechanism of energy dissipation, and the absence of damage. This is also consistent with friction measurements on CVD graphene by others, which showed that much higher contact stresses and a much higher number of cycles are needed to damage CVD graphene. ⁴⁷ Based on previous MD simulations, ^{12, 14} it is possible that the squeeze-out of hydration layers could be related to the abrupt increase in friction at ~60 nN in Figure 3. Therefore, in the velocity-dependent friction-force measurements discussed next, the load was maintained smaller than 20 nN (~5 GPa) to avoid this transition from happening.



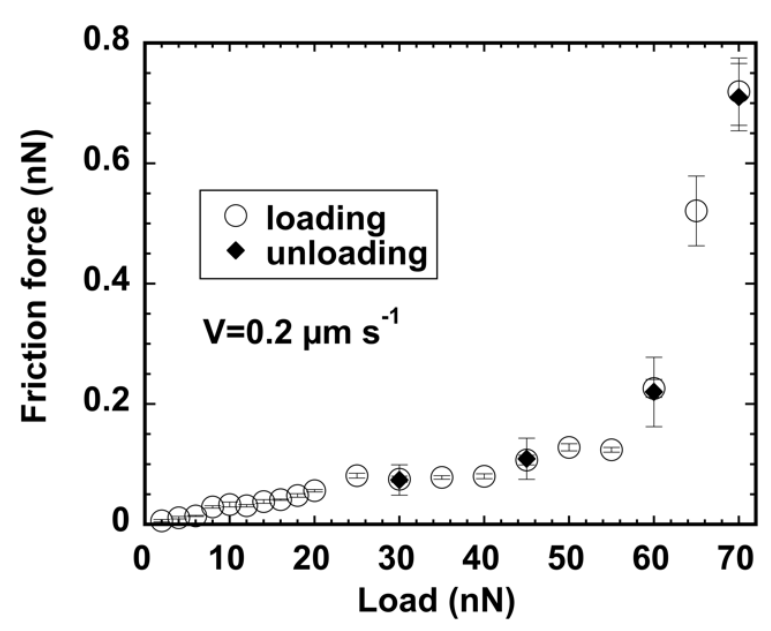


Figure 3. Friction force between the AFM tip and graphene as a function of load at constant sliding velocity of $0.2 \ \mu m \ s^{-1}$ measured while the load is gradually increased (loading, empty circles) and decreased (unloading, filled diamonds). Tip radius is 34 nm. Cartoon.

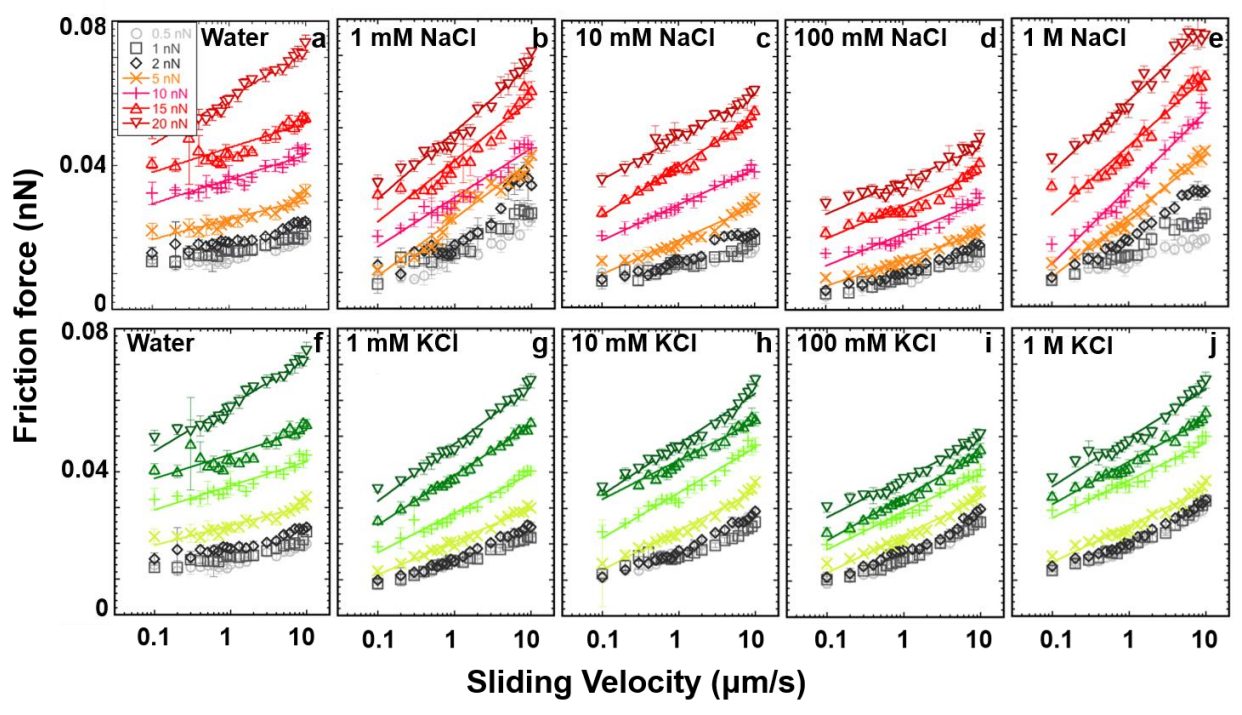


Figure 4. Friction force between graphene and the AFM tip as a function of velocity and normal load. Measurements were taken in NaCl (a-e, shades of red) and KCl (f-j, shades of green) solutions at the concentrations of (a, f) 0 mM (water), (b, g) 1 mM, (c, h) 10 mM, (d, i) 100 mM, and (e, j) 1 M, at a pH of 6.0±0.2. Error bars give the variation in friction across eight friction loops. Light grey, grey, and black represent applied loads of 0.5, 1, and 2 nN respectively, while the colored shade from light to dark (in red for NaCl and in green for KCl) indicates applied loads from 5 to 20 nN (see legend in a). According to Hertzian contact mechanics, the average stress ranges from 1.3 to 4.3 GPa for loads between 0.5 nN and 20 nN, given a tip radius of 34 nm. A magnification of the results at loads from 0.2 nN to 2 nN is shown in Figure S8. The solid lines show the fits of Eq. 1-2 to the experimental results.

Figure 4 shows representative results of the friction force, $F_{\rm L}$, between graphene and the tip as a function of the sliding velocity, V, and at loads ranging from 0.5 to 20 nN in water and in NaCl and KCl solutions at the selected concentrations. It is evident that friction increases with both load

and velocity under all investigated conditions. Further, friction decreases with addition of salt down to a minimum at a concentration of 100 mM, and it increases in 1 M solutions, especially in the case of NaCl. The electrolyte concentration has an intricate effect on the slope and intercepts of the friction *vs.* velocity curves, which will be analyzed later. The reference measurements on the underlying Si/SiO₂ substrate in aqueous solutions feature (i) much higher friction compared to graphene and (ii) a pronounced decrease in friction with velocity throughout the whole range of investigated sliding velocities (Figure S7), which indicates that the mechanism of frictional dissipation in Figure 4 is greatly determined by the graphene surface.

Shear-assisted thermally activated slip theory

The friction-force measurements are evaluated in the light of the shear-assisted thermally activated slip theory. We treat the molecular slip along the slip plane as a rate process in the context of Eyring's theory, 49-50 in which a shear force applied on the molecule couples with its thermal energy to increase the rate of flow or slip. For slip to occur, the molecule, initially in an equilibrium position (an energy minimum), needs to pass over an energy barrier E_a (the transition state) before reaching the adjacent energetic minimum. The applied shear force on the molecule has the effect of lowering this energy barrier by $F_L\lambda$, which increases the slip rate. λ is the shear-activation length and represents the displacement of the molecules from the energetic minimum to the transition state, 48 as shown in Figure 5a. Considering that the slip rate of the water molecules, ν , is increased by the applied shear force according to $\nu \sim \nu^* \exp(-(E_a - F_L\lambda)/k_BT)$, k_B being the Boltzmann constant, T the absolute temperature and ν^* the vibration frequency in a reference state, the following expression is obtained for the shear force F_L :52

$$F_L = \frac{E_a}{\lambda} + \frac{k_B T}{\lambda} \ln(V/V_0)$$

328 Eq. (1)

 $V = d \cdot v$ being the sliding velocity, d the hopping distance of the molecules and $V_0 = d \cdot v^*$ a reference velocity.

Many experimental and computational studies have showed that the shear stress between two surfaces with a lubricant film scales with the logarithmic of the sliding velocities; see recent review. In some of these works, the influence of the pressure (P) was additionally considered. For instance, Evans and Briscoe considered the effect an increase in the energy barrier, sa-54 i.e. $E_a + P \cdot \Omega$, where Ω is the so-called pressure-activation volume. Since both the contact area and the distribution of forces among the confined molecules are unknown, we refrain from describing the slip rate process in terms of pressure and activation volumes, and instead, we consider the increase of the energy barrier as $E_a + L \cdot \gamma$, where L is the load and γ a pressure-activation length; this approach was followed in a recent AFM study of the oxidation of graphene driven by the tip force. Here, $L \cdot \gamma$ represents the work applied to move the molecules vertically away from the surface a distance γ against the applied pressure (like a dilation), which is required for slip to happen. This leads to a modified model for the shear force:

$$F_L = \frac{E_a + L \cdot \gamma}{\lambda} + \frac{k_B T}{\lambda} \ln(V/V_0)$$

344 Eq. (2)

The linear relation between energy barrier and the normal load assumes that the structure and compliance of the molecules does not change during the sliding process. Although more complex models to describe the change of the energy barrier with load are possible,⁵¹ a linear relation leads to regression coefficients better than 0.95 here, and hence, it is sufficient. Eq. 2 thus accounts for the effects of pressure and shear stress on the molecular slip of a fluid film of a few nanometers in thickness, with slip rate: $\nu \sim \nu^* \exp(-(E_a + L \cdot \gamma - F_L \lambda)/k_B T)$. Note that the parameters λ and γ

are defined for the total applied normal load and shear force in the confined liquid films, respectively, and not for the force applied on a single molecule, as in Eyring's original model.

The logarithmic dependence of the measured friction force with the sliding velocity in Figure 4 is consistent with Eqs. 1-2, and the lines represent the fits to this model. At a specific load, the slope of each F_L vs. V curve gives λ , while $\Sigma = E_a + L \cdot \gamma - k_B T \cdot \ln(V_0)$ is obtained from the intercept. The slope of Σ vs. L gives γ and the intercept provides $E_a - k_B T \cdot \ln(V_0)$. In order to unambiguously determine E_a , it is necessary to determine the reference velocity V_0 , for which we have performed separate temperature-dependent friction-force measurements. Figure S9 shows that the friction force (at constant velocity of 1 μ m/s) decreases linearly with increasing temperature for each specific load, as expected for a thermally activated process and from Eq. 2. Figure S10 confirms this trend for another series of experiments as a function of the sliding velocity, load and temperature. It is noted that the range of accessible temperatures in our AFM is very narrow (25-50°C), which hinders a precise determination of V_0 , but the average value of 40 m/s is reasonable considering the residence time of water molecules in bulk solution and in the hydration shell of ions (~10⁻¹¹ s ⁵⁶); see SI for detailed information about V_0 .

Shear activation length and thermal activation energy

The obtained fitting parameters (λ , γ and E_a) are summarized in Figure 5. It is evident that λ decreases significantly with increasing normal load from ~2.5 to 1 nm (Figure 5d-e), which likely results from the increase in the area by ~4.5 with the increase in load from ~2 to 20 nN.⁵⁵ Reference tests on mica give λ values ranging from ~0.9 to 0.2 nm for water (Figure S11), and therefore, much smaller than for graphene, meaning that, under shear, water sticks to mica more than to graphene. This is consistent with the greater slip length of water on graphene compared to mica.⁵⁷

The addition of 1mM NaCl and KCl causes an abrupt decrease in the shear-activation length (Figures 5d and 5e), *i.e.* the molecules slip less easily than in pure water. Note that Figure 6b only shows results at loads ≥ 2 nN in NaCl solutions, because a power law often describes these results better than a logarithmic function (Figure S8).

The change of λ is ion- and concentration-specific. The change of the shear-activation length with NaCl concentration is intricate: there is an initial decrease when 1mM NaCl is added to the solution (similar to 1mM KCl), but further increase in concentration leads to an elongation of the activation length, and a concentration of 1M NaCl causes λ to significantly contract again, indicating that there are several competing mechanisms at play. In contrast, the shear-activation length in KCl is less dependent on concentration. This electrolyte-specific response of λ may be related to the different composition of the confined fluid films. The layer-size distribution in NaCl solutions suggested the presence of interfacial water and of Na⁺ with multiple hydration states, while less water and less hydrated ions were present in the KCl films (inset in Figure 2). We thus speculate that the variation of the shear-activation length reflects the different hydration states of the cations, with higher values associated to greater amounts of water in the fluid film. With an increase in NaCl concentration, more Na⁺ ions increasingly populate the fluid film; these ions are more strongly hydrated, which leads to an increase in the amount of confined water in the thin films. The dramatic decrease in λ in 1M NaCl coincides with the increase in adhesion and in the presence of layers with less hydrated Na⁺ ions, as described earlier.

394

393

374

375

376

377

378

379

380

381

382

383

384

385

386

387

388

389

390

391

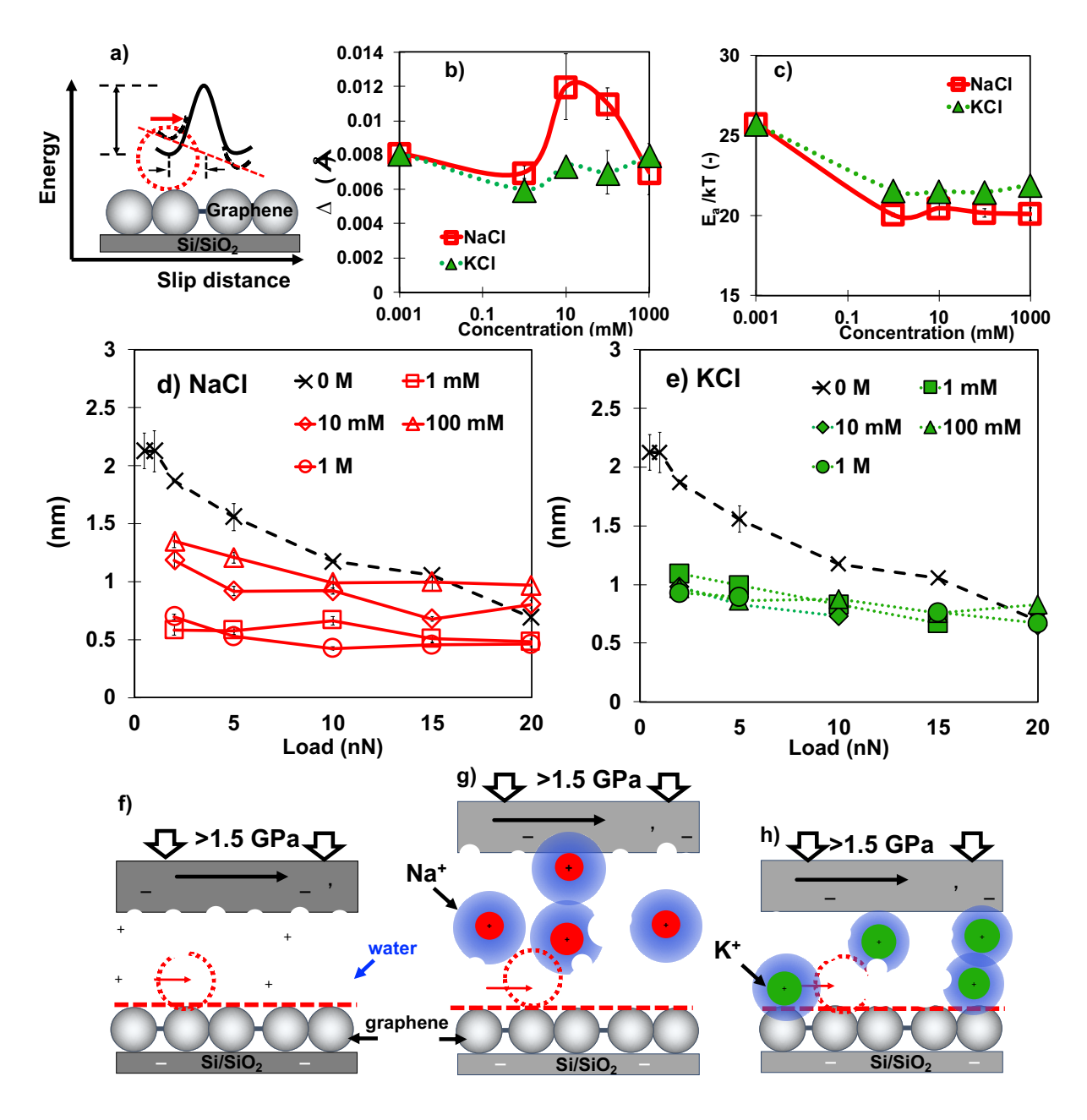


Figure 5. (a) Illustration of the shear-assisted thermally activated slip in films of aqueous solutions confined between an AFM tip and the graphene surface. (b) Thermal activation energy (E_a/k_BT) , (c) displacement along the normal direction $(\Delta \gamma)$, and (d-e) shear-activation length (λ) in water, (d) NaCl and (e) KCl solutions. The error bars show the root-mean-square errors of the fits and they are often smaller than the symbol size, and, therefore, not always visible. The cartoons show the molecular slip (f) in water and in 10 mM (g) NaCl and (h) KCl solutions. In 10 mM NaCl, the

Na⁺ ions retain larger amounts of water than in KCl at the same concentration. The graphene is represented by the grey carbon atoms above the Si/SiO₂ substrate. The red dashed line shows the proposed location of the slip plane. In the electrolyte solutions, the observed change in λ could also imply a change of the slip plane location, but the low surface charge supports that the electrostatic attraction of ions to the surface is weak, and therefore, we speculate that it is still located at the graphene surface.

The ions significantly reduce the thermal activation energy from $\sim 26~k_BT$ to $\sim 20~k_BT$ and $\sim 21~k_BT$ in KCl and NaCl solutions, respectively (Figure 5b). Based on Eyring's slip theory, the thermal activation energy for slip arises from the distortion of the interactions with the molecules in neighboring layers, *i.e.* here, the hydrogen bond network between the interfacial water layers and the interaction strength between the water molecules and the surface. The presence of the ions is known to disturb the hydrogen bond network of the interfacial water, ⁵⁸ which justifies that the molecular slip requires lesser thermal activation energy in the electrolyte solutions than in pure water. Ion-specific effects are reflected in the pressure-activation length of the confined films: note that γ increases with NaCl concentration and it abruptly decreases in 1M NaCl, while it remains approximately constant in KCl. The higher dilation seen at intermediate NaCl concentrations might be also associated to the higher amounts of retained water by the confined Na⁺ ions in the thin films, but more studies are needed to understand these results.

Comparisons to literature are limited to surfactant monolayers and polymers confined by different solid surfaces. For example, reported values for Langmuir-Blodgett monolayers on mica are: ${}^{54}E_a \sim 26 \ k_B T$ and shear-activation volume (instead of "length", λ) $\sim 3.3-5 \ \text{nm}^3$, *i.e.* larger than the molecular volume of the surfactant $\sim 0.5 \ \text{nm}^3$, which was interpreted as a cooperative or collective motion of 5-10 molecules. We have obtained a very similar thermal activation energy

and a smaller shear-activation volume of $\sim \lambda \cdot A_{mol} \sim 0.11$ nm³ for $\lambda = 2$ nm in pure water ($A_{mol} = area$ of water molecule), perhaps due to the smaller size of the molecules in this work. While the two systems are chemically different, and hence, a quantitative comparison is not targeted here, the results are of the same order of magnitude.

429

430

431

432

433

434

435

436

437

438

439

440

441

442

443

444

445

446

447

425

426

427

428

Discussion

Several works have reported electrolyte-specific graphene properties, which are consistent with an ion-specific composition of the graphene/solution interface. For instance, the conductance of graphene in liquid-gated transistors is strongly affected by changes in ionic strength, pH and the type of ions present, which has been proposed to rely on changes of the electrical double layer.³⁵ This work has scrutinized the electrical double layer on graphene supported on Si/SiO₂ substrate for two electrolytes at various concentrations and pH values. As inferred from the OHP potential, distinct Stern layers form on the graphene surface as a function of the electrolyte composition, which is attributed to the different adsorption strengths of hydronium, potassium and sodium ions. Applying high pressures (≥0.5 GPa) with an AFM tip against the graphene surface enables the confinement of an aqueous film of nanometer thickness (<3 nm) that is composed of layers of water molecules as well as ions, which maintain the electroneutrality of the system. The normal force measurements allowed us to partially resolve the structure of these thin films with subnanometer resolution. The prominent difference between the structure of the confined aqueous films is proposed to rely on the higher hydration strength of the Na⁺ ions, which remain further away from the surface and retain more water in their hydration shells compared to K⁺.

The friction between the AFM tip and graphene was evaluated in the light of the shear-assisted thermally activated slip theory, which provided insight into the molecular slippage. In the case of

pure water, Figure 5g shows two layers of water molecules but there might be more, along with a small concentration of hydronium to maintain electroneutrality; here, it was assumed that the surface charges are ~ 2 nm apart (\sim -0.3 nm⁻²). While the upper wall moves laterally at constant velocity, the water molecules and some hydronium slip along the graphene plane. A large shear-activation length λ implies that the molecules are not pinned to the surface under shear, thereby also leading to a large slip length. The ease of the water molecules to slip is reflected in the large shear-activation length on graphene compared to mica (Figure S11), consistent with the greater slip length of water on graphene. ^{18,57}

As deduced from the significant decrease in λ with addition of only 1mM salt, it appears that a small amount of Na⁺ and K⁺ ions is sufficient to "stick" water to the graphene. Figures 5h and 5i illustrate two aqueous films at intermediate concentrations, when slippage is favored in NaCl solution compared to KCl. The sensitivity of slippage to the electrolyte composition implies that both cations and anions must populate the films; note that the concentration of cations cannot be increased without including sufficient anions in order to maintain electroneutrality. The observed ion-specific effects on the slippage are consistent with the hydration strength of the cations: strongly hydrated Na⁺ ions retain more water in the confined films and do not penetrate the hydration layers, which promotes slippage. Note that higher amounts of trapped Na⁺ ions (and anions) at higher NaCl concentrations should retain more water, which would be consistent with the observed increase in shear-activation length. This does not happen in the case of K+, a weaker hydrated cation. These results corroborate previously observed phenomena of varying mobility of hydrated ions in confined configurations such as through carbon nanotubes and induced swelling of multilayer graphene and graphene oxide membranes. ⁵⁹⁻⁶⁰ Furthermore, these findings indicate

that tuning the ionic solution composition can be a strategy to modulate the molecular slippage in graphene nanochannels.

The implications of this work for the tribological performance of graphene in an aqueous environment are discussed next. Here, the origin of friction is the irreversible work dissipated (F_L . λ) when the molecules fall from the transition state to the adjacent energetic minimum. It appears that the addition of an electrolyte to pure water causes a reduction of the thermal activation energy and of the shear-activation length at several concentrations, both results *conversely* affecting the friction force; note that the overall change in friction in Figure 4 appears to be small, so that, interestingly, both changes partially compensate each other. The lowest friction is attained at a concentration of 100 mM in both salts, which indicates that, here, the effect of the ions on lowering the thermal activation energy dominates over the slippage along the graphene surface. One intriguing result is that at the highest NaCl concentration (1M), the "sticking" effect to the graphene seems to take over, as shown by the higher increase in friction compared to KCl at the same concentration. This, however, cannot be rationalized based on our simple model. It is possible that atomic-scale roughness introduced via the confinement of ions contributes to this result. However, proving this hypothesis requires consideration of other theories and models that are out of the scope of this work. Finally, while the structural superlubricity of graphene may be impaired by the presence of water, as proved in theory, ¹⁵ our results suggest that a proper selection of electrolyte may be used to tune the lubricious properties of graphene, when water is present in the system.

25

470

471

472

473

474

475

476

477

478

479

480

481

482

483

484

485

486

487

488

489

490

491

Conclusions

493

494

495

496

497

498

499

500

501

502

503

504

505

506

507

508

509

510

511

This study demonstrates that modulating the electrolyte composition may be a means to control the molecular slip, and thus, fluid flow through graphene nanochannels, as well as friction at graphene contacts in an aqueous environment. Graphene interacts with molecules and ions in its close vicinity via the delocalized π -electrons, and hence, molecular adsorption is sensitive to graphene doping. 61-62 Given the relevance of the adsorption strength of the liquid molecules to the surface on the considered slip-rate process, the present study opens a new avenue of research about how modulating the electronic properties of graphene could be used to tune the interfacial motion of fluids, the flow in graphene nanochannels, and friction in the presence of a lubricant film. While we will examine the effects of substrate-induced doping of graphene on molecular slippage and friction in the near future, the effects of the pH and temperature on these phenomena still remain open questions that also need to be addressed. Further, we have shown that the measurement of normal and lateral forces can provide a conceptual understanding of the graphene-electrolyte interface. This type of studies can also be extended to probe the influence of adsorbed/intercalated ions on/underneath graphene on the transport properties of solution-gated graphene FETs and on interfacial properties of semiconducting 2D transition metal dichalcogenides. Characterization of 2D supercapacitor electrode surfaces via this approach may also enable identification (at the subnanometer level) of the relative contributions of ion adsorption versus Faradic mechanisms, for both aqueous and non-aqueous electrolytes, including ionic liquids.

512

513

514

Methods

Graphene synthesis

Monolayer graphene was synthesized via low-pressure chemical vapor deposition on 25μm copper foils using methane as the precursor with hydrogen/argon carrier gas as previously documented. The graphene samples were transferred onto ~285 nm thick thermally-grown silicon oxide on silicon wafers (Nova Electronic Materials) using poly(bisphenol A carbonate) handle layers (1.5 wt% in chloroform, MW ~45kDa) by solution etching of the copper substrate (0.1M sodium persulphate, Sigma-Aldrich). As-prepared samples were subsequently annealed at 500°C in a hydrogen/argon environment to improve graphene-substrate adhesion and to remove surface and interfacial polymeric residue immediately prior to measurements.

Sample preparation

Sodium chloride (NaCl) and potassium chloride (KCl) (purity>=99.0%, Sigma-Aldrich) were dissolved at room temperature in ultrapure water (18.2 M Ω -cm resistivity) to achieve concentrations of 0 mM (no salt added), 1 mM, 10 mM, 100 mM, and 1 M. The pH of the solutions was adjusted to 3.0, 6.0, and 9.0±0.2 through incremental addition of HCl and NaOH solutions. Muscovite mica substrates for reference tests were prepared by manually cleaving ruby mica of optical quality Grade #1 (S&J Trading, Inc.) just before the AFM experiments. Reference experiments were performed on the freshly cleaved mica and on a naturally oxidized silicon wafer (p-type Boron <111> 500 μ m, WRS) that was cleaned with toluene, isopropanol, and ethanol, and UV-ozone treated prior to the immersion into the investigated solution.

Normal and friction force measurement

A Nanowizard AFM (JPK Instruments) located in an acoustic chamber was used throughout this study. The samples were fixed in a homemade fluid-cell with 2 ml of solution. The cell was

covered by a membrane to minimize evaporation of the electrolyte solutions. To exchange the solution every time, a syringe was used to deplete the previous electrolyte solution in the mounted fluid-cell, which was then refilled with the next investigated solution with another syringe with extreme caution. This process was repeated for three times to ensure a thorough exchange of the electrolyte solution. After 1-hour equilibration in each solution at 25°C, normal and lateral forces were measured with AFM cantilevers (CSC38/no Al, Mikromasch) having spring constants of 0.1-0.3 N/m, as determined by the thermal calibration method.⁶³ The lateral sensitivities were determined in each experiment based on the method described in ref ⁶⁴. The tip used in the experiments shown here has a radius of ~34 nm, as determined by Scanning Electron Microscopy imaging. Reproducibility was confirmed by replica experiments with different tips. Prior to the force measurements, several regions were imaged in contact mode after equilibration in water for 2 hours to select relatively large areas (\sim 5 μ m x 5 μ m) far away from defects and boundaries. Short tests were conducted on the selected regions to ensure the absence of "pucker-up" effects in friction loops,65 which was interpreted as a good adhesion of the graphene to the underlying Si/SiO2 substrate and was critical for the success of the force measurements. Each sample was divided into two halves with a diamond pen and each half was used for the measurements with DI water and with one of the salts. All friction-force measurements with the same electrolyte were conducted within the same region to ensure that the sliding direction with respect to the crystal lattice orientation was maintained constant during each series of experiments with a particular salt. Isothermal lateral force measurements were performed as a function of load (L) and velocity (V)at each selected concentration with a sliding length of 100 nm. The highest applied load was 20 nN, which yields a pressure of 4.3 GPa, assuming a Hertzian contact radius of 1.2 nm -calculated with elastic moduli of 155 and 1000 GPa and Poisson ratios of 0.2 and 0.17 for silicon and

538

539

540

541

542

543

544

545

546

547

548

549

550

551

552

553

554

555

556

557

558

559

graphene, respectively. Force-separation curves were collected at an approach speed of 20 nm s⁻¹. The thickness of the steps and the pull-off force were obtained from the analysis of 256 curves per concentration for each electrolyte and for water. Structural changes of the graphene surface and of the tip (wear) did not occur under the conditions of our experiments. Force measurements on a single graphene sample took 10-12 hours, during which the system was observed to remain stable. The friction-force measurements were conducted by sliding the tip along a fixed length of 100 nm (~8 traces and retraces for a single data point). Considering that the drift of our instrument is ~2 nm per 1 hr and that the slowest scan takes ~1 s (2 s for trace and retrace), the drift can be considered to have a negligible effect, and so the tip slides along the same line. The small error bars that give the friction force averaged over ~8 friction loops support that the properties of graphene do not gradually change during the sliding process. Temperature-dependent friction-force measurements were performed using the same JPK Nanowizard AFM as the rest of the experiments, but the standard sample stage and fluid cell were replaced with the JPK PetriDishHeater/PetriDishHolder. The Si/SiO₂ substrates beneath the graphene samples were glued to 9.2 cm² TPP tissue culture dishes (Techno Plastic Products). Friction experiments were performed at 25° C (room temperature), 30° C, 35° C, 40° C, 45° C, and 50° C in 1 mM NaCl. The setup was allowed to thermally equilibrate for 30 minutes before each set of measurements. The temperature setpoint to achieve the selected temperatures was determined from a calibration experiment in pure water, in which setpoint and heater temperature (measured by the JPK) were compared to the manually measured temperature in the solution. During the calibration, the AFM was in a powered-on state but did not have a cantilever attached to the cantilever holder and was not actively scanning. The calibration was performed over the course of 60 minutes at various

561

562

563

564

565

566

567

568

569

570

571

572

573

574

575

576

577

578

579

580

581

582

temperatures between room temperature and 50° C. Figure S12 demonstrates that an initial equilibration period of ~15 minutes is required to achieve constant temperature. The calibration provided the setpoint temperature required to achieve the selected temperatures in the solution, which is key to model the temperature dependent friction-force measurements using Eqs. 1-2.

ASSOCIATED CONTENT

Supporting Information. Discussion of the DLVO model, surface forces between tip and graphene in KCl solution at large and small distances and as a function of the pH in water and in 1mM, reference surface-force measurements on mica, PAH, and Si/SiO₂, reference friction-force measurements on mica and Si/SiO₂, friction between tip and graphene at loads ≤ 2 nN, temperature-dependent friction force between graphene and tip and temperature calibration.

596 AUTHOR INFORMATION

Corresponding Author

*Rosa M. Espinosa-Marzal, Tel: +1 217 607 3856, E-mail address: rosae@illinois.edu

Author Contributions

§ Both authors have contributed equally to this work

ACKNOWLEDGEMENT

We would like to thank J. Lopez-Berganza for developing the code used to process the friction data. S. Nam gratefully acknowledges support from the NSF DMR-1708852.

1. Novoselov, K. S.; Geim, A. K.; Morozov, S. V.; Jiang, D.; Zhang, Y.; Dubonos, S. V.; Grigorieva, I. V.; Firsov, A. A., Electric field effect in atomically thin carbon films. *Science* **2004**,

609 *306* (5696), 666-9.

Huang, X.; Yin, Z.; Wu, S.; Qi, X.; He, Q.; Zhang, Q.; Yan, Q.; Boey, F.; Zhang, H., Graphene-based materials: synthesis, characterization, properties, and applications. *Small* **2011**, *7*

612 (14), 1876-902.

- 3. Du, X.; Skachko, I.; Barker, A.; Andrei, E. Y., Approaching ballistic transport in suspended graphene. *Nat Nanotechnol* **2008**, *3* (8), 491-5.
- Lee, C.; Wei, X.; Kysar, J. W.; Hone, J., Measurement of the elastic properties and intrinsic strength of monolayer graphene. *Science* **2008**, *321* (5887), 385-8.
- 5. Kim, K. S.; Lee, H. J.; Lee, C.; Lee, S. K.; Jang, H.; Ahn, J. H.; Kim, J. H.; Lee, H. J., Chemical vapor deposition-grown graphene: the thinnest solid lubricant. *ACS Nano* **2011**, *5* (6),

619 5107-14.

- 620 6. Dienwiebel, M.; Verhoeven, G. S.; Pradeep, N.; Frenken, J. W. M.; Heimberg, J. A.; Zandbergen, H. W., Superlubricity of Graphite. *Physical Review Letters* **2004**, *92* (12), 126101.
- 622 7. Hone, J.; Carpick, R. W., Friction. Slippery when dry. Science **2015**, 348 (6239), 1087-8.
- 8. Ashraf, A.; Wu, Y.; Wang, M. C.; Aluru, N. R.; Dastgheib, S. A.; Nam, S., Spectroscopic investigation of the wettability of multilayer graphene using highly ordered pyrolytic graphite as

625 a model material. *Langmuir* **2014**, *30* (43), 12827-36.

9. Li, Z.; Wang, Y.; Kozbial, A.; Shenoy, G.; Zhou, F.; McGinley, R.; Ireland, P.; Morganstein, B.; Kunkel, A.; Surwade, S. P.; Li, L.; Liu, H., Effect of airborne contaminants on

the wettability of supported graphene and graphite. *Nat Mater* **2013**, *12* (10), 925-31.

- 10. Schrader, M. E., Ultrahigh vacuum techniques in the measurement of contact angles. IV. Water on graphite (0001). *J. Phys. Chem.* **1975**, *79* (23), 2508-2515.
- 631 11. Berman, D.; Deshmukh, S. A.; Sankaranarayanan, S. K.; Erdemir, A.; Sumant, A. V., Friction. Macroscale superlubricity enabled by graphene nanoscroll formation. *Science* **2015**, *348* (6239), 1118-22.
- 12. Vilhena, J. G.; Pimentel, C.; Pedraz, P.; Luo, F.; Serena, P. A.; Pina, C. M.; Gnecco, E.; Perez, R., Atomic-Scale Sliding Friction on Graphene in Water. *ACS Nano* **2016**, *10* (4), 4288-93.
- 13. Robinson, B. J.; Kay, N. D.; Kolosov, O. V., Nanoscale interfacial interactions of graphene with polar and nonpolar liquids. *Langmuir* **2013**, *29* (25), 7735-42.
- 14. Ye, Z.; Egberts, P.; Han, G. H.; Johnson, A. T.; Carpick, R. W.; Martini, A., Load-Dependent Friction Hysteresis on Graphene. *ACS Nano* **2016**, *10* (5), 5161-8.
- Lee, H.; Ko, J. H.; Choi, J. S.; Hwang, J. H.; Kim, Y. H.; Salmeron, M.; Park, J. Y., Enhancement of Friction by Water Intercalated between Graphene and Mica. *J Phys Chem Lett* **2017**, 8 (15), 3482-3487.
- 16. Thompson, P. A.; Robbins, M. O.; Grest, G. S., Structure and Shear Response in Nanometer-Thick Films. *Isr. J. Chem.* **1995**, *35* (1), 93-106.
- 17. Urbakh, M.; Klafter, J.; Gourdon, D.; Israelachvili, J., The nonlinear nature of friction. *Nature* **2004**, *430* (6999), 525-8.
- 647 18. Ortiz-Young, D.; Chiu, H. C.; Kim, S.; Voitchovsky, K.; Riedo, E., The interplay between apparent viscosity and wettability in nanoconfined water. *Nat Commun* **2013**, *4*, 2482.

649 19. Savage, R. H., Graphite Lubrication. J. Appl. Phys. **1948**, 19 (1), 1-10.

- 650 20. Levita, G.; Restuccia, P.; Righi, M. C., Graphene and MoS2 interacting with water: A comparison by ab initio calculations. *Carbon* **2016**, *107*, 878-884.
- Cohen-Tanugi, D.; Grossman, J. C., Water desalination across nanoporous graphene. *Nano Lett.* **2012**, *12* (7), 3602-8.
- Radha, B.; Esfandiar, A.; Wang, F. C.; Rooney, A. P.; Gopinadhan, K.; Keerthi, A.;
- Mishchenko, A.; Janardanan, A.; Blake, P.; Fumagalli, L.; Lozada-Hidalgo, M.; Garaj, S.; Haigh,

- S. J.; Grigorieva, I. V.; Wu, H. A.; Geim, A. K., Molecular transport through capillaries made with atomic-scale precision. *Nature* **2016**, *538* (7624), 222-225.
- 658 23. Majumder, M.; Chopra, N.; Andrews, R.; Hinds, B. J., Nanoscale hydrodynamics:
- enhanced flow in carbon nanotubes. *Nature* **2005**, *438* (7064), 44.
- Huang, D. M.; Sendner, C.; Horinek, D.; Netz, R. R.; Bocquet, L., Water slippage versus contact angle: a quasiuniversal relationship. *Phys Rev Lett* **2008**, *101* (22), 226101.
- 25. Xie, Q.; Alibakhshi, M. A.; Jiao, S.; Xu, Z.; Hempel, M.; Kong, J.; Park, H. G.; Duan, C., Fast water transport in graphene nanofluidic channels. *Nat Nanotechnol* **2018**, *13* (3), 238-245.
- 664 26. Celebi, A. T.; Barisik, M.; Beskok, A., Surface charge-dependent transport of water in graphene nano-channels. *Microfluidics and Nanofluidics* **2017**, *22* (1), 7.
- Kannam, S. K.; Todd, B. D.; Hansen, J. S.; Daivis, P. J., Slip length of water on graphene:
- Limitations of non-equilibrium molecular dynamics simulations. *J Chem. Phys* **2012**, *136* (2), 024705.
- 669 28. Israelachvili, J. N., *Intermolecular and Surface Forces*. Elsevier Science: 2011.
- 670 29. Iler, R. K., The chemistry of silica. Wiley, New York: 1979.
- 671 30. Yin, J.; Zhang, Z.; Li, X.; Yu, J.; Zhou, J.; Chen, Y.; Guo, W., Waving potential in graphene. *Nat Commun* **2014**, *5*, 3582.
- 51. Zachariah, Z.; Espinosa-Marzal, R. M.; Heuberger, M. P., Ion specific hydration in nanoconfined electrical double layers. *J. Colloid Interface Sci.* **2017**, *506* (Supplement C), 263-270.
- 32. Schlegel, M. L.; Nagy, K. L.; Fenter, P.; Cheng, L.; Sturchio, N. C.; Jacobsen, S. D., Cation sorption on the muscovite (001) surface in chloride solutions using high-resolution X-ray reflectivity. *Geochimica et Cosmochimica Acta* **2006**, *70* (14), 3549-3565.
- 33. Pashley, R. M., Dlvo and Hydration Forces between Mica Surfaces in Li+,Na+,K+,and Cs+ Electrolyte-Solutions a Correlation of Double-Layer and Hydration Forces with Surface Cation-Exchange Properties. *J. Colloid Interface Sci.* **1981,** 83 (2), 531-546.
- Williams, C. D.; Dix, J.; Troisi, A.; Carbone, P., Effective Polarization in Pairwise Potentials at the Graphene-Electrolyte Interface. *J Phys Chem Lett* **2017**, 8 (3), 703-708.
- 683 35. Heller, I.; Chatoor, S.; Mannik, J.; Zevenbergen, M. A.; Dekker, C.; Lemay, S. G., Influence of electrolyte composition on liquid-gated carbon nanotube and graphene transistors. *J. Am. Chem. Soc.* **2010**, *132* (48), 17149-56.
- 686 36. Chen, F.; Qing, Q.; Xia, J.; Li, J.; Tao, N., Electrochemical gate-controlled charge transport in graphene in ionic liquid and aqueous solution. *J. Am. Chem. Soc.* **2009**, *131* (29), 9908-9.
- Shi, G.; Ding, Y.; Fang, H., Unexpectedly strong anion-pi interactions on the graphene flakes. *J. Comput. Chem.* **2012**, *33* (14), 1328-37.
- 690 38. Emami, F. S.; Puddu, V.; Berry, R. J.; Varshney, V.; Patwardhan, S. V.; Perry, C. C.; Heinz, 691 H., Force Field and a Surface Model Database for Silica to Simulate Interfacial Properties in
- 692 Atomic Resolution. *Chem. Mater.* **2014**, *26* (8), 2647-2658.
- 693 39. Sharma, P.; Miskovic, Z. L., Ionic screening of charged impurities in electrolytically gated graphene: A partially linearized Poisson-Boltzmann model. *J. Chem. Phys.* **2015**, *143* (13), 695 134118.
- 696 40. Chen, F.; Xia, J.; Tao, N., Ionic screening of charged-impurity scattering in graphene. *Nano Lett.* **2009**, *9* (4), 1621-5.
- 41. Israelachvili, J. N.; Pashley, R. M., Molecular Layering of Water at Surfaces and Origin of Repulsive Hydration Forces. *Nature* **1983**, *306* (5940), 249-250.
- 700 42. Kilpatrick, J. I.; Loh, S. H.; Jarvis, S. P., Directly probing the effects of ions on hydration forces at interfaces. *J. Am. Chem. Soc.* **2013**, *135* (7), 2628-34.
- 43. Espinosa-Marzal, R. M.; Drobek, T.; Balmer, T.; Heuberger, M. P., Hydrated-ion ordering in electrical double layers. *Phys Chem Chem Phys* **2012**, *14* (17), 6085-93.
- 704 44. Smith, D. W., Ionic hydration enthalpies. *Journal of Chemical Education* **1977**, *54* (9), 705 540.
- 706 45. Jiang, G. P.; Cheng, C.; Li, D.; Liu, J. Z., Molecular dynamics simulations of the electric
- double layer capacitance of graphene electrodes in mono-valent aqueous electrolytes. *Nano Research* **2016**, *9* (1), 174-186.

- 709 46. Kjellander, R.; Marcelja, S., Correlation and Image Charge Effects in Electric Double-710 Layers. *Chemical Physics Letters* **1984**, *112* (1), 49-53.
- Peng, Y.; Wang, Z.; Zou, K., Friction and Wear Properties of Different Types of Graphene
- Nanosheets as Effective Solid Lubricants. *Langmuir* **2015**, *31* (28), 7782-91.
- 48. Spikes, H.; Tysoe, W., On the Commonality Between Theoretical Models for Fluid and Solid Friction, Wear and Tribochemistry. *Tribol. Lett.* **2015**, *59* (1), 21.
- 715 49. Eyring, H., The activated complex in chemical reactions. *J. Chem. Phys.* **1935,** *3* (2), 107-716 115.
- 50. Eyring, H., Viscosity, plasticity, and diffusion as examples of absolute reaction rates. *J. Chem. Phys.* **1936**, *4* (4), 283-291.
- 51. Spikes, H., Stress-augmented thermal activation: Tribology feels the force. *Friction* **2018**, 720 6(1), 1-31.
- 721 52. Ma, L.; Gaisinskaya-Kipnis, A.; Kampf, N.; Klein, J., Origins of hydration lubrication. *Nat Commun* **2015**, *6*, 6060.
- 53. Lichter, S.; Martini, A.; Snurr, R. Q.; Wang, Q., Liquid slip in nanoscale channels as a rate process. *Phys Rev Lett* **2007**, *98* (22), 226001.
- 54. Briscoe, B.; Evans, D. In *The shear properties of Langmuir-Blodgett layers*, The Royal Society: 1982; pp 389-407.
- 727 55. Raghuraman, S.; Elinski, M. B.; Batteas, J. D.; Felts, J. R., Driving Surface Chemistry at the Nanometer Scale Using Localized Heat and Stress. *Nano Lett.* **2017**, *17* (4), 2111-2117.
- 729 56. Chowdhuri, S.; Chandra, A., Molecular dynamics simulations of aqueous NaCl and KCl solutions: Effects of ion concentration on the single-particle, pair, and collective dynamical properties of ions and water molecules. *J Chem. Phys* **2001**, *115* (8), 3732-3741.
- 57. Bonaccurso, E.; Kappl, M.; Butt, H.-J., Hydrodynamic Force Measurements: Boundary Slip of Water on Hydrophilic Surfaces and Electrokinetic Effects. *Physical Review Letters* **2002**, 88 (7), 076103.
- 735 58. Cafolla, C.; Voitchovsky, K., Lubricating properties of single metal ions at interfaces. *Nanoscale* **2018**, *10* (25), 11831-11840.
- 737 59. Choi, W.; Ulissi, Z. W.; Shimizu, S. F.; Bellisario, D. O.; Ellison, M. D.; Strano, M. S., Diameter-dependent ion transport through the interior of isolated single-walled carbon nanotubes.
- 739 Nat Commun **2013**, 4, 2397.
- 740 60. Abraham, J.; Vasu, K. S.; Williams, C. D.; Gopinadhan, K.; Su, Y.; Cherian, C. T.; Dix, J.; Prestat, E.; Haigh, S. J.; Grigorieva, I. V.; Carbone, P.; Geim, A. K.; Nair, R. R., Tunable sieving of ions using graphene oxide membranes. *Nat. Nanotechnol.* **2017**, *12* (6), 546-+.
- Huttmann, F.; Martinez-Galera, A. J.; Caciuc, V.; Atodiresei, N.; Schumacher, S.; Standop, S.; Hamada, I.; Wehling, T. O.; Blugel, S.; Michely, T., Tuning the van der Waals Interaction of
- Graphene with Molecules via Doping. *Physical Review Letters* **2015**, *115* (23), 236101.
- 746 62. Schumacher, S.; Wehling, T. O.; Lazic, P.; Runte, S.; Forster, D. F.; Busse, C.; Petrovic, M.; Kralj, M.; Blugel, S.; Atodiresei, N.; Caciuc, V.; Michely, T., The backside of graphene: manipulating adsorption by intercalation. *Nano Lett.* **2013**, *13* (11), 5013-9.
- 749 63. Hutter, J. L.; Bechhoefer, J., Calibration of atomic- force microscope tips. *Rev. Sci.* 750 *Instrum.* **1993**, *64* (7), 1868-1873.
- 751 64. Mullin, N.; Hobbs, J. K., A non-contact, thermal noise based method for the calibration of lateral deflection sensitivity in atomic force microscopy. *Rev. Sci. Instrum.* **2014**, *85* (11), 113703.
- 753 65. Li, Q. Y.; Lee, C.; Carpick, R. W.; Hone, J., Substrate effect on thickness-dependent
- friction on graphene. *Physica Status Solidi B-Basic Solid State Physics* **2010**, 247 (11-12), 2909-2914.